Power delivery and self-heating in nanoscale near field transducer for heat-assisted magnetic recording

2015 Nanotechnology 26 134001

(http://iopscience.iop.org/0957-4484/26/13/134001)

IOP Publishing Nanotechnology
Nanotechnology **26** (2015) 134001 (7pp) doi:10.1088/0957-4484/26/13/134001

Power delivery and self-heating in nanoscale near field transducer for heat-assisted magnetic recording

Nan Zhou, Luis M Traverso and Xianfan Xu

School of Mechanical Engineering and Birck Nanotechnology Center, Purdue University, West Lafayette, IN, USA 47907

E-mail: xxu@purdue.edu

Received 4 November 2014, revised 13 January 2015
Accepted for publication 15 January 2015
Published 11 March 2015

Abstract

To keep increasing the storage density in next-generation hard disk drives, heat-assisted magnetic recording is being developed where a nanoscale near field transducer (NFT) locally and temporally heats a sub-diffraction-limited region in the recording medium to reduce the magnetic coercivity. This allows the use of very small grain in the medium while still maintaining data thermal stability. Plasmonic nanostructures made of apertures or antennas are good candidates for NFTs because of their capability of subwavelength light manipulation in optical frequencies. The NFT must simultaneously deliver enough power to the recording medium with as small as possible incident laser power to reduce self-heating in the NFT, which could cause thermal expansion and materials failure that lead to degradation of the overall hard drive performance. In this work, we study the effect of optical properties on the power delivery efficiency of nanoscale bowtie aperture antennas, with the presence of a recording media stack. Heat dissipation and temperature rise in the NFT are also computed to investigate their dependence on materials' properties. The possibility of using alternative plasmonic materials for delivering higher power and/or reducing heating in NFTs is discussed.

Keywords: near field optics, nanoscale optical antenna, heat assisted magnetic recording

(Some figures may appear in colour only in the online journal)

1. Introduction

Driven by 40% annual growth in the need for worldwide data storage, increase in areal density, expressed in bits per square inch, is crucial for the hard disk drive (HDD) industry. The conventional perpendicular magnetic recording (PMR) technology is not likely to advance the areal density beyond 1 Tb in^{-2} because of the superparamagnetic limit [1]. As the grain volume in the recording medium shrinks to make the bits more closely packed, the medium must have high coercivity to maintain thermal stability, which exceeds the currently available magnetic write fields. Heat-assisted magnetic recording (HAMR) is a promising technique for advancing the areal density beyond 1 Tb in^{-2} by incorporating local heating using near field optics [2–4]. Significant progress in HAMR has been made [5–8], and companies in the HDD industry are on the verge of introducing the HAMR technology into products within the next few years, as indicated in the roadmap from the Advanced Storage Technology Consortium (ASTC) in figure 1 [9].

In figure 2 we illustrate the concept of the HAMR technology. The key component is a near field transducer (NFT) that provides local heating to the recording media to lower its coercivity, which removes the switching limitation in PMR. The design of NFTs, usually in the form of an optical antenna that includes an aperture-type antenna, is primarily based on excitation of surface plasmons (SP) and/or localized surface plasmon (LSP) resonance of a nanostructure, which generates an intense sub-diffraction-limited light spot on the magnetic medium [10]. Note that for 1 Tb in^{-2}, the required mark length is about 50 nm with a bit aspect ratio of 4.0, about 16 times smaller than the 800 nm

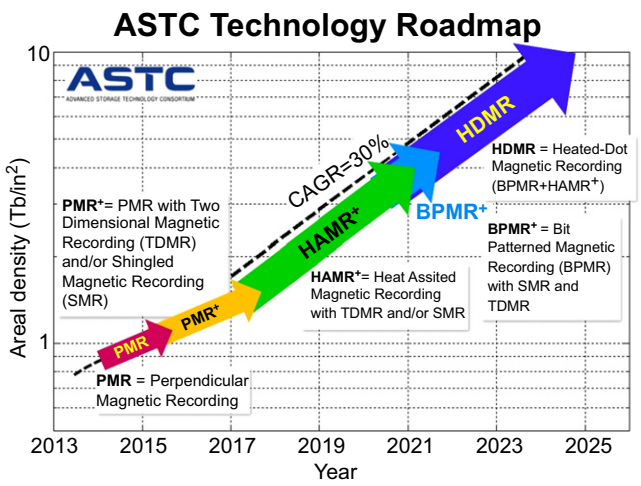

Figure 1. ASTC Technology Roadmap. CAGR: compound annual growth rates.

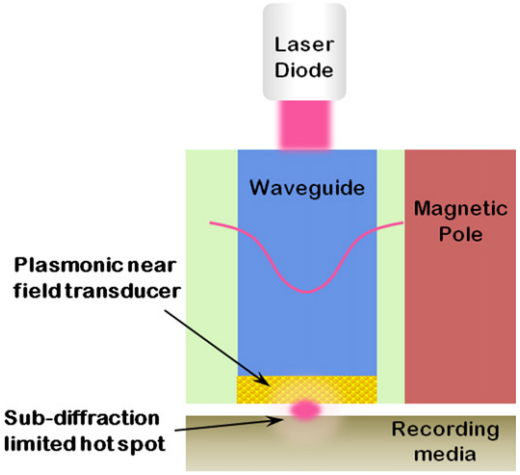

Figure 2. Illustration of the HAMR concept.

wavelength of a diode laser that can be economically used for HAMR. Apart from localizing the laser beam to a spot less than 50 nm, the NFT must simultaneously deliver enough power to the recording medium with as small as possible incident laser power to reduce the possible self-heating. Thus, the coupling efficiency of an NFT is a key figure of merit in determining the quality for a given transducer design.

Thermal issues significantly impact the stability of materials and components, which degrades the overall performance of an HDD [5, 10–12]. Made of plasmonic materials, mostly metallic materials, the temperature in an NFT can rise by several hundred degrees because of the self-heating effect [13]. The NFT can protrude to the recording media surface because of the thermal expansion. To avoid contact between the NFT and the medium surface, the air gap and the surface roughness have to be better controlled [5]. The temperature rise also changes the distance between the NFT and the writing pole, which may attenuate the resonance of the NFT since the writing pole is part of the resonance structure. Approaches to address the heating issue include engineering NFT materials, improving thermal properties of

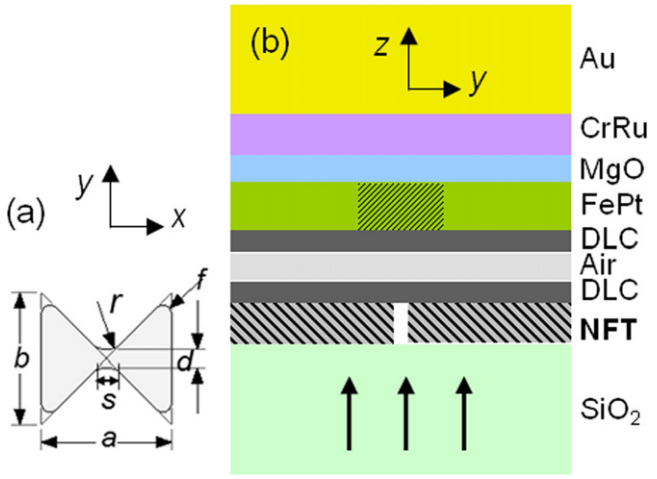

Figure 3. (a) The geometry of the bowtie aperture and (b) the material stack, including the recording media.

the media stack, and changing the heating scheme [10]. In this work, we investigate the effect of optical properties on the power delivery efficiency and self-heating in NFTs in the shape of bowtie apertures by carrying out both electromagnetic (EM) and thermal simulations. The figure of merit of the bowtie aperture NFT, which in this work is defined as the ratio of the temperature rise in the media to that in the NFT, is quantitatively related to the real and imaginary parts of the optical constant. The possibility of using alternative plasmonic materials for delivering higher power and/or reducing heating in NFTs will be discussed.

2. Simulation model

2.1. EM simulations

We performed numerical simulations using ANSYS HFSS, a commercial frequency-domain finite-element method (FEM) solver. The three-dimensional structure is subdivided into tetrahedral elements. A solution is found for the fields within the finite elements, and the fields are interrelated so that Maxwell's equations are satisfied across inter-element boundaries. Figure 3 illustrates a bowtie aperture in the *xy* plane and the simulation model in the *yz* plane. Bowtie apertures are good examples for generating confined optical spots with high transmission by combining the plasmonic effect, the lightning-rod phenomenon at sharp tips, and the propagating waveguide mode that enhances optical transmission, which have been extensively studied [14–16]. As shown in figure 3(a), the small air gap was simulated by two closely spaced rounded tips with a curvature of r, which form a gap size of s and d that determines the localization capability primarily. The symbol f represents the rounded corners in an actual manufactured bowtie aperture. The aperture was centered in the simulation model. The model had a size of $3000 \times 3000\ \text{nm}^2$ in the *xy* plane. Radiation boundaries were applied to the exterior surfaces to create an open model. A denser mesh, with an average edge length of 3 nm, was used

Table 1. Thicknesses and optical properties of the material stack. (DLC: diamond-like carbon)

Material	Thickness [nm]	n	k
Au	50	0.154	4.908
CrRu	15	3.15	5.68
MgO	5	1.76	0
FePt	8	3.3	4.3
Lower DLC	1	1.53	0
Air	2	1	0
Upper DLC	1	1.53	0
NFT	t	—	—
SiO_2	∞	1.453	0

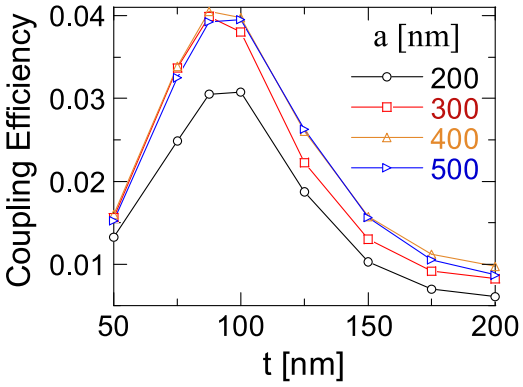

Figure 4. Coupling efficiency as a function of the dimension a and thickness t for a gold bowtie aperture with s = d = 5 nm.

inside and in the vicinity of the bowtie aperture. The composition, thicknesses, and optical properties of the material stack are listed in table 1, where the thickness and properties for the NFT film will be varied in this study. The optical properties for Au [17] and SiO_2 [18] were evaluated at 800 nm wavelength. Properties of other materials were provided by ASTC. A normally incident Gaussian beam at 800 nm wavelength, polarized along the y-direction, was applied to excite the aperture from the substrate side as indicated by the arrows in figure 3(b). The peak electric field amplitude in free space was 1 V m^{-1}. The optical coupling efficiency was computed as the fraction of the input power dissipated in an 80 nm-diameter cylinder (as indicated by the shaded region, 8 nm thick) in an FePt layer, where the dissipated power density q (volumetric loss density) is expressed as

$$q = 1/2\,\mathrm{Re}(\sigma)\,|E|^2 = 1/2\varepsilon_0\omega\,\mathrm{Im}(\varepsilon)\,|E|^2. \quad (1)$$

Here σ is the conductivity, ε is the relative permittivity, and $\varepsilon = 1 + i\sigma/\varepsilon_0\omega$ [19]. ε_0 is the vacuum permittivity, and ω is the angular frequency.

2.2. Thermal modeling

After calculating the field intensity and thus the dissipated power density from the EM numerical simulation, we can input this data into a thermal simulation model. We constructed a numerical thermal model using Mechanical ANSYS, which is also an FEM solver. The thermal analysis was based on solving the temperature T using the heat conduction equation for differential control volumes, which can be described by the following equation:

$$\rho c\left(\frac{\partial T}{\partial t}\right) = \ddot{q} + \frac{\partial}{\partial x}\left(k_x\frac{\partial}{\partial x}\right) + \frac{\partial}{\partial y}\left(k_y\frac{\partial}{\partial y}\right) + \frac{\partial}{\partial z}\left(k_z\frac{\partial}{\partial z}\right). \quad (2)$$

where ρ is the density of the volume, k is the thermal conductivity, and $\ddot{q}$ is the volumetric heat input into the element. On the coordinates of the nodes corresponding to the mesh in the thermal model, we interpolated the scaled values of the volumetric loss density. The scaled volumetric loss density (W/m^3) then became the heat generation input in the thermal model in which we computed the increase in temperature in both the NFT and the recording medium. The elemental control volume had dimensions of 6 nm corresponding to the regions of higher heat generation gradient such as in the gap-metal interface and the heated region on the recording medium. Inside the heated region the shape of the elements was brick, whereas the shape of the outer elements was made tetrahedral. To simulate a large thermal reservoir, a large volume around the heated region was constructed to make sure that the heated region would reach a steady state. In both EM and thermal modelings, the model was sliced in four parts and only one part was computed, taking advantage of the symmetry of the geometry. Since EM models were made by normalizing the value of the peak input field to 1 V m^{-1}, we scaled heat generation in the thermal model to values corresponding to appropriate focused laser intensity. Here we considered an 800 nm wavelength laser beam with a total power of 40 mW focused to a waist of 0.3 μm, with a heating duration of 1 ns, which is approximately the time period that a given spot is heated during operation. Pulses were assumed to be delivered as constant values within the pulse duration by maintaining volumetric heat generation values constant. The temperature rises in both the media and the NFT are scalable with the input power, and 40 mW was used here to raise the temperature in the FePt above the Curie temperature. With the calculated temperatures in the NFT and FePt layers, we computed the thermal efficiency figure of merit, which is defined as the ratio of maximum nodal temperature change in the recording medium to that in the NFT:

$$\text{Thermal Efficiency} = \frac{\Delta T_{peak\ in\ media}}{\Delta T_{peak\ in\ NFT}}. \quad (3)$$

3. Results and analysis

As indicated in equation (1), dissipation in a lossy material scales linearly with both the imaginary part of the permittivity Im(ε) and the field intensity |E|^2 that is primarily determined by the real part of the permittivity Re(ε). Generally, a large

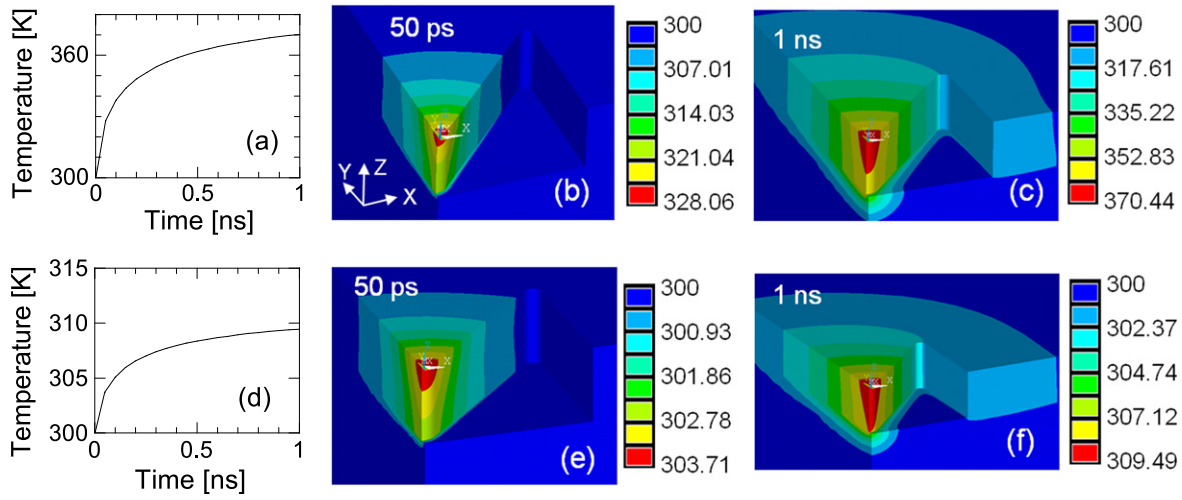

Figure 5. (a), (d) Temporal and (b), (c), (e), (f) spatial temperature distributions in NFT film for a gold (top row) and silver (bottom row) bowtie aperture NFT.

magnitude of $-\mathrm{Re}(\varepsilon)$ (more negative $\mathrm{Re}(\varepsilon)$) indicates a strong resonance, large field enhancement, and lateral energy confinement, which is favorable for an NFT in the HAMR application. On the other hand, to minimize self-heating in NFT, $\mathrm{Im}(\varepsilon)$ and $|E|^2$ should be reduced according to equation (1). Therefore there is a compromise between improving field localization/enhancement and minimizing heating. For a diode laser at near-infrared wavelengths, silver suffers from chemical stability, although it has the smallest $\mathrm{Im}(\varepsilon)$ in the wavelength range of a diode laser and a relatively large $-\mathrm{Re}(\varepsilon)$. Gold is widely used as the NFT material because of its chemical stability, a large melting point, and high thermal conductivity. As an illustration, we use both gold and silver as the NFT material for this study.

3.1. Optical and thermal modeling of gold and silver bowtie aperture NFT

We first perform a comparative study between gold and silver bowtie apertures, with known optical [17] and thermal properties from literature [20]. The suitability of using bowtie apertures as NFTs has been studied [3, 10, 16]. In figure 4 we show the coupling efficiency for a gold bowtie aperture at various dimensions and thicknesses, at the excitation wavelength of 800 nm. The incident Gaussian beam has a waist of 0.3 μm, which is close to the focused source in a real HAMR head [3, 6]. The best coupling efficiency with $s = d = 5$ nm is about 4.1% for $a = 400$ nm and $t = 87.5$ nm. The corresponding full-width at half-maximum spot size in FePt is about 19×19 nm^2 (not shown). The film thickness affects the coupling efficiency by introducing Fabry–Perot resonances. If one keeps increasing the thickness, more peaks will appear [16]. Changing the aperture outline dimension affects the effective propagation constant as well as the impedance, where the aperture defined in metal film can be considered as a short section of waveguide [21]. A relatively large impedance mismatch between the aperture and the recording media causes lower coupling efficiency for $a = 200$ nm, as shown in figure 4. We also see that the coupling efficiency only slightly varies with the gap size d [16], and for a larger gap of $s = d = 20$ nm, the spot size is about 40×40 nm^2 with a 3.92% coupling efficiency. For the rest of the work, we will fix the dimensions at $a = 400$ nm, $t = 90$ nm, and $s = d = 20$ nm, which is a physically more realizable gap size.

The calculated dissipated power density was exported from the EM calculation and used as the heat source for thermal modeling. For the maximum temperature node, the temperature as a function of time is shown in figures 5(a) and (d) for bowtie apertures in gold and silver films, respectively. Temperature distributions in the bowtie apertures at 50 ps and 1 ns are also shown in figures 5(b) and (c) for gold film, and in figures 5(e) and (f) for silver film. The temperature distribution at 50 ps corresponds to the beginning of heating and the heat dissipation effect is small; therefore it also represents the distribution of absorbed laser energy. Figure 5 shows that in the gold film, the temperature increases quickly at first and then starts to saturate. At 50 ps and 1 ns, the peak temperature occurs at the tip of the bowtie aperture where the field enhancement and absorption are most intense. For the same bowtie aperture made in silver film, the temporal and spatial temperature distributions are quite similar, but with a much smaller magnitude. The corresponding temperature evolution of the maximum temperature node and distributions in the FePt media are shown in figures 6(a) to (c) for gold aperture and in figures 6(d) to (f) for silver aperture, which indicate comparable temperature rises.

Table 2 summarizes the performance of gold and silver bowtie aperture NFTs, including the coupling efficiency, the absorption rate (dissipation normalized to the total input power), the peak temperature rises in NFTs, and the FePt media when heated for 1 ns. The silver NFT provides a slightly better coupling efficiency, which leads to a slightly higher peak rise ΔT in the recording media. On the other hand, with a much smaller imaginary part of the permittivity, the absorption rate in the silver film is much smaller. This has a direct effect on the smaller peak ΔT in the silver

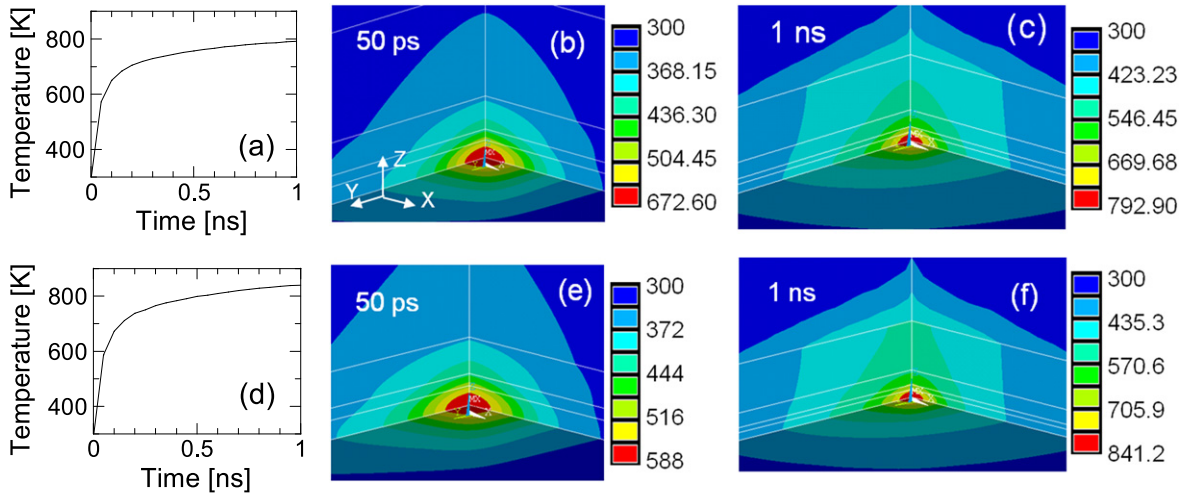

Figure 6. (a), (d) Temporal and (b), (c), (e), (f) spatial temperature distributions in the recording medium FePt for a gold (top row) and silver (bottom row) bowtie aperture NFT.

Table 2. Comparable study of gold and silver bowtie aperture NFT.

Material	Permittivity (800 nm)	Coupling efficiency	Absorption rate in NFT film	Peak ΔT in NFT	Peak ΔT in FePt	Thermal efficiency
Gold	−24.06 + i1.52	4.04%	6.97%	70.4	492.9	7.0
Silver	−30.98 + i0.4	4.37%	1.28%	9.5	541.2	57.0

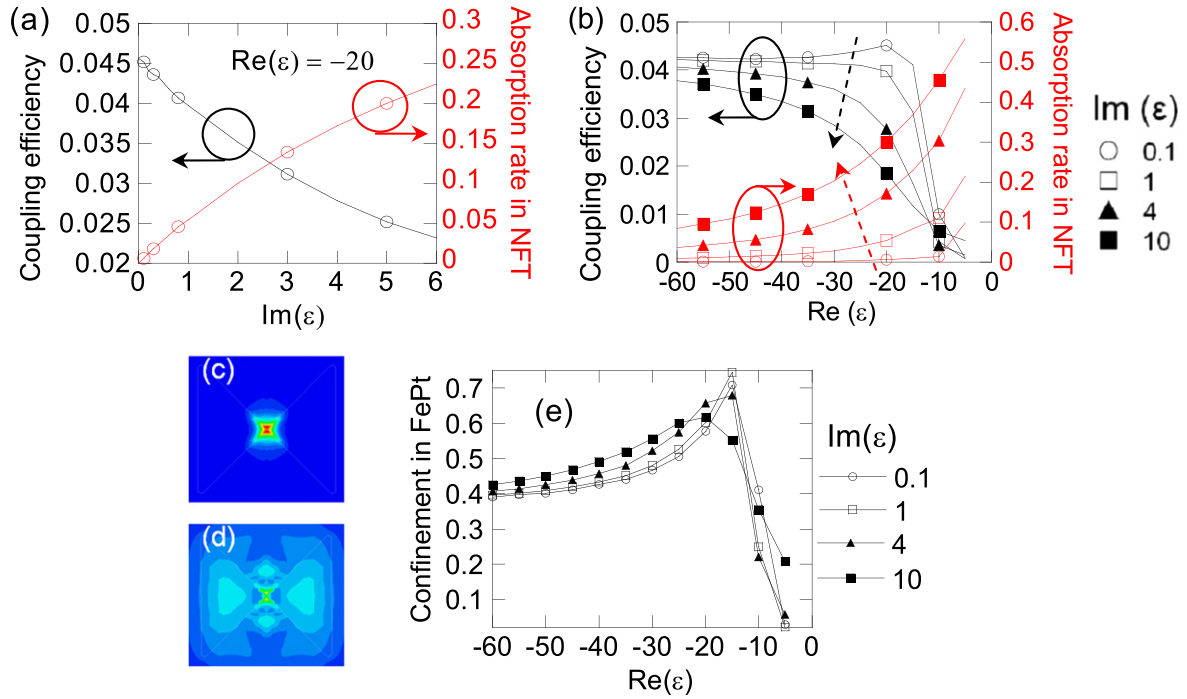

Figure 7. Parametric study of the effect of permittivity on coupling efficiency (black lines) and absorption rate in an NFT (red lines) as a function of (a) Im(ε) and (b) Re(ε). Field distributions in FePt with (c) Re(ε) = −20 and Im(ε) = 0.1, (d) Re(ε) = −5, and Im(ε) = 0.1. Note that in (d) the field strength has been multiplied 20 times to compare with (c). (e) Dependence of the confinement in FePt on the permittivity.

NFT. Finally, we calculated the thermal efficiency defined in equation (3) and shown in table 2, which indicates that silver provides a thermal efficiency about eight times that of gold.

3.2. Using alternative plasmonic materials

Materials engineering is always important for improving the performance of devices [22]. For HAMR application, investigating alternative materials holds the promise of lowering the self-heating in NFTs, which is commonly made in gold, and/or of improving the thermal robustness of materials [23–25]. Here we conduct a parametric study to gain insight into the dependence of NFT performance on optical constants. Figure 7 shows the influence of optical properties of NFT materials on the coupling efficiency and the absorption rate in an NFT. If the real part of the permittivity is fixed at −20, we can see from figure 7(a) that the absorption rate in an NFT (red curves) increases almost linearly with Im(ε), the same as predicted by equation (1). Consequently, the coupling efficiency decreases. The dependence on Re(ε) is given in figure 7(b), considering four values of Im(ε). With a negligible loss (e.g., Im (ε) = 0.1), there exists an optimized Re(ε) for the best coupling efficiency. But generally, a relatively large |Re(ε)| is preferred to produce better coupling efficiency and smaller dissipation in an NFT. From the point view of circuit theory, changing optical properties of NFT materials varies the effective impedance to match/mismatch that of the media stack [21]. The best coupling efficiency in figure 7(b) is about 4.52%, with Re(ε) = −20 and Im(ε) = 0.1, and the corresponding absorption rate in the NFT is as low as 0.61%. The absorption profile in the media stack is shown in figure 7(c) with a spot size of 36.5 (x) × 38.5 (y) nm^2. The results in figure 7(b) are consistent with equation (1), which implies that |Re(ε)| cannot be too small. As demonstrated by the field distribution with Re(ε) = −5 and Im(ε) = 0.1 in figure 7(d), light is not localized if the material does not have a large enough |Re(ε)|. To quantitatively characterize the confinement in FePt, we plot in figure 7(e) the fraction of the absorbed power in the entire FePt layer that dissipated in the central 80 nm-diameter cylinder. As indicated in figure 7(d), with Re(ε) = −5 and Im(ε) = 0.1, the power spreads and only less than 3% is confined in a region of 80 nm diameter.

4. Conclusion

We report the dependence of the power delivery efficiency and self-heating in NFTs on optical properties. By carrying out EM and thermal simulations of bowtie aperture NFTs with the presence of a recording media stack, we perform a comparative study between gold and silver NFTs. The results demonstrate that with a much smaller imaginary part of the permittivity, silver provides a thermal efficiency eight times that of gold. Parametric studies of permittivity further indicate that it is promising to simultaneously deliver higher power and reduce heating in NFTs by engineering materials with as small as possible loss and a moderate real part of the permittivity.

Acknowledgments

The authors gratefully acknowledge the support of the Defense Advanced Research Projects Agency (Grant No. N66001-08-1-2037), the National Science Foundation (Grant No. CMMI-1120577), and the Advanced Storage Technology Consortium (ASTC).

References

[1] Sharrock M P 1990 *IEEE Trans. on Mag.* **26** 193–7
[2] Rottmayer R E *et al* 2006 *IEEE Trans. on Mag.* **42** 2417–21
[3] Challener W A, Gage E, Itagi A and Peng C 2006 *Jpn. J. Appl. Phys.* **45** 6632–42
[4] O'Connor D and Zayats A V 2010 *Nat. Nanotechnol.* **5** 482–3
[5] Challener W A *et al* 2009 *Nat. Photon* **3** 220–4
[6] Stipe B C *et al* 2010 *Nat. Photon* **4** 484–8
[7] Kong Y, Chabalko M, Black E, Powell S, Bain J A, Schlesinger T E and Luo Y 2011 *IEEE Trans. on Mag.* **47** 2364–7
[8] Maletzky T, Zhou D, Jin E X and Dovek M 2014 *Proc. of SPIE* **9201** 92010J
[9] ASTC Technology Roadmap—2014 v8, The Advanced Storage Technology Committee of the International Disk Equipment and Materials Association, San Jose, California, USA, Sept. 2, 2014 (www.idema.org/?page_id=5868)
[10] Zhou N, Xu X, Hammack A T, Stipe B C, Gao K, Scholz W and Gage E C 2014 *Nanophotonics* **3** 141–55
[11] Xu B X, Liu Z J, Ji R, Toh Y T, Hu J F, Li J M, Zhang J, Ye K D and Chia C W 2012 *J. Appl. Phys.* **111** 07B701
[12] Evans R F L, Chantrell R W, Nowak U, Lyberatos A and Richter H-J 2012 *Appl. Phys. Lett.* **100** 102402
[13] Xu B, Toh Y T, Chia C W, Li J, Zhang J, Ye K and An C 2012 *IEEE Trans. on Mag.* **48** 1789–93
[14] Jin E X and Xu X 2006 *Appl. Phys.* B **84** 3–9
[15] Challener W A and Itagi A V 2009 Near-field optics for heat-assited magnetic recording (experiment, theory, and modelling) *Modern Aspects of Electrochemistry Modelling and Numerical Simulation II No*. 44 53–111 (New York: Springer)
[16] Zhou N, Kinzel E C and Xu X 2011 *Appl. Opt.* **50** G42–6
[17] Johnson P B and Christy R W 1972 *Phys. Rev.* B **6** 4370–9
[18] Palik E D 1998 *Handbook of Optical Constants of Solid* (San Diego: Academic)
[19] Maier S A 2007 *Plasmonics: Fundamentals and Applications* (New York: Springer)
[20] The thermal properties for DLC were taken from Shamsa M, Liu W L, Balandin A A, Casiraghi C, Milne W I and Ferrari A C 2006 *Appl. Phys. Lett.* **89** 1–3
For air, Ag, Au, and SiO_2, thermal properties are from www.engineeringtoolbox.com
For CrRu, the same engineering toolbox website was used to find the properties of the elements Cr and Ru, then calculated using an atomic weighted average
For MgO, thermal properties are from www.azom.com/properties.aspx?ArticleID=54
The thermal properties for FePt were taken from Chernyshov A, Treves D, Le T, Zong F, Ajan A and Acharya R 2014 *J. Appl. Phys.* **115** 1–3

[21] Itagi A V, Stancil D D, Bain J A and Schlesinger T E 2003 *Appl. Phys. Lett.* **22** 4474–6
[22] Boltasseva A and Atwater H A 2011 *Science* **331** 290–1
[23] Zhu M, Zhao T, Riemer S C and Kautzky M C 2013 *Patent* US2013/0286799 A1
[24] Zhao T, Kautzky M C, Challener W A and Seigler M A 2013 *Patent* US8427925 B2
[25] Zhao T, Sahoo S, Kautzky M C and Itagi A V 2013 *Patent* US2013/0279315 A1